Geochemistry Geophysics Geosystems G3
AN ELECTRONIC JOURNAL OF THE EARTH SCIENCES
Published by AGU and the Geochemical Society

Article
Volume 8, Number 3
8 March 2007
Q03004, doi:10.1029/2006GC001440
ISSN: 1525-2027

A ridgelet transform method for constraining tectonic models via abyssal-hill morphology

Nathan J. Downey and Robert W. Clayton

Seismological Laboratory, California Institute of Technology, 1200 East California Boulevard, 252-21, Pasadena, California 91125, USA (ndowney@gps.caltech.edu)

[1] Abyssal-hill shape and orientation are related to the direction and spreading rate of paleo-spreading centers. Therefore analyzing abyssal-hill shape and trend is useful for constraining tectonic models of regions devoid of magnetic reversal anomalies. Detecting systematic changes of abyssal-hill shapes or trends, due to changes in spreading rate or direction, is not straightforward, which makes it difficult to determine appropriate regions over which to average abyssal-hill parameters. Often, however, detecting these systematic changes, where they occur, and the scale over which they occur, is of primary importance for tectonic reconstructions. We present a new method of abyssal-hill analysis that is based on the ridgelet transform, a relative of the two-dimensional wavelet transform. Our method is capable of locally estimating the width, azimuth, and root-mean-square (RMS) amplitude of abyssal-hill fabric and highlights changes in these parameters across a survey area, making it possible to identify regions created with a constant spreading rate and direction. We use three multibeam swaths, one crossing the Osbourn Trough in the southwest Pacific Basin, one crossing the East Pacific Rise, and one crossing the Mid-Atlantic Ridge, to demonstrate the utility and performance of our method.

Components: 6876 words, 9 figures, 1 table.

Keywords: ridgelet transform; abyssal hills.

Index Terms: 0520 Computational Geophysics: Data analysis: algorithms and implementation.

Received 3 August 2006; **Revised** 21 November 2006; **Accepted** 8 December 2006; **Published** 8 March 2007.

Downey, N. J., and R. W. Clayton (2007), A ridgelet transform method for constraining tectonic models via abyssal-hill morphology, *Geochem. Geophys. Geosyst.*, *8*, Q03004, doi:10.1029/2006GC001440.

1. Introduction

[2] Measurements of abyssal-hill morphology can be used to constrain tectonic histories of regions devoid of magnetic reversal anomalies [*Menard*, 1967]. By examining the shape and orientation of abyssal hills over these regions, it is possible to make spreading rate and direction estimates for use in tectonic reconstructions; however, other factors can also affect abyssal-hill shape and trend [*Goff et al.*, 1997].

[3] The shape of abyssal hills is controlled by the faulting process that occurs at oceanic spreading centers after the formation of oceanic crust [*Buck and Polikov*, 1998; *Goff et al.*, 1995; *Macdonald et al.*, 1996]. The nature of this faulting is determined by the local stress state, which is in turn, related to the spreading rate. Therefore several measures of abyssal-hill shape correlate with spreading rate and direction. These measures include abyssal-hill width, asymmetry (measured as a difference in slope between the sides facing toward and away from the spreading center) and root-mean-square

(RMS) amplitude [*Goff*, 1991; *Goff et al.*, 1997; *Hayes and Kane*, 1991; *Kriner et al.*, 2006]. Abyssal-hill trend (the azimuth of the hill's long axis) and the distribution in azimuths of the slopes facing toward and away from the spreading axis are useful indicators of paleo-spreading direction [*Goff and Jordan*, 1988; *Kriner et al.*, 2006].

[4] Abyssal-hill shape and azimuth naturally vary. Even amongst abyssal hills simultaneously created at a single spreading center there is a slight variation in these parameters. This natural variation therefore requires that we obtain an average abyssal-hill shape that can then be used to infer spreading rates and directions. This variation makes it necessary to use statistical tests to determine if the mean shape or trend of two populations of abyssal hills is different. The techniques of *Goff and Jordan* [1988] and *Kriner et al.* [2006] approach the problem of abyssal-hill variation by estimating an average shape and trend parameter for a region of seafloor. During this process, any systematic change in abyssal-hill shape across this region is lost, making it necessary to use a cross-validation approach, where several estimates are made over the same area using different estimation regions, to determine the location of systematic changes in abyssal-hill shape. Often, however, these changes are interesting tectonic features, that indicate a change in spreading rate or direction. For example, *Larson et al.* [2002] were able to map the location of the Pacific-Phoenix-Farallon triple junction trace by examining changes in abyssal-hill trends.

[5] In this paper we present a new method of estimating the width, trend, and RMS amplitude of abyssal hills based on the ridgelet transform [*Candès*, 1998; *Starck et al.*, 2002, 2003]. This method is spatially local, with the capability of determining the shape and azimuth of individual abyssal hills. The advantage of this technique is that averaging after shape estimation makes it easier to identify the location of systematic changes in abyssal-hill shape. As a result, determining appropriate regions over which to average shapes and azimuths is simplified. We demonstrate the usefulness of this technique by examining three swaths of multibeam data (Figure 1), one collected near the Osbourn Trough (OT) [*Lonsdale*, 1997], one collected near the East Pacific Rise (EPR) and one collected near the Mid-Atlantic Ridge (MAR). Our results highlight the differences between abyssal hills created at fast and slow spreading centers, as outlined by *Goff* [1991], *Goff et al.* [1995, 1997], and *Hayes and Kane* [1991]. We are able to detect two regions of anomalous seafloor morphology near the EPR, which correspond to the location of the Louis Scarp and Yaquina Fracture Zone [*Eakins and Lonsdale*, 2003] and are able to show that the Louis Scarp marks the location of a possible change in spreading direction. We also identify the possible location of either a change in the spreading direction of the Osbourn paleo-spreading center or the location of a triple junction trace, and the location of a possible reduction of spreading rate at the Osbourn paleo-spreading center.

2. Ridgelet Transform

2.1. Wavelet Analysis of Geologic Textures

[6] The two-dimensional ridgelet transform [*Candès*, 1998; *Starck et al.*, 2003] is a relative of the two-dimensional wavelet transform. Wavelet transform methods have varied application in the Earth sciences [*Kumar and Foufoula-Georgiou*, 1997], including quantifying the multiscale alignment of fault outcrops in a continental setting [*Ouillion*, 1996], the study of rock fabric alignment [*Gaillot et al.*, 1999], and the analysis of seafloor texture [*Little et al.*, 1993]. *Little et al.* [1993] used one-dimensional (1-D) wavelets to highlight a region of reduced short-wavelength power and enhanced long-wavelength power in a center-beam bathymetry profile collected northeast of Hawaii. They conclude that this anomalous region was created at a small abandoned spreading center, which they were able to locate near the region's center. The wavelet transform allowed them to separate the scales of the bathymetry so that a large-scale

Figure 1. (a) Basemap outlining the locations of the Osbourn Trough (OT), East Pacific Rise (EPR), and Mid-Atlantic Ridge (MAR) multibeam data sets used in this study. (b) The solid line in this figure marks the location of the Osbourn Trough multibeam swath. The data collected along the yellow section of this line are plotted in Figure 3a. (c) Same as Figure 1b except for the East Pacific Rise data set. The three yellow sections of the EPR swath are plotted in Figures 5a–5c. (d) The location of the Mid-Atlantic Ridge multibeam swath, the yellow section of which marks the location of the multibeam data plotted in Figure 6. The dashed lines in Figures 1b–1d mark the locations of active spreading centers (EPR and MAR) or, in the case of the OT data set, the location of the extinct Osbourn spreading center.

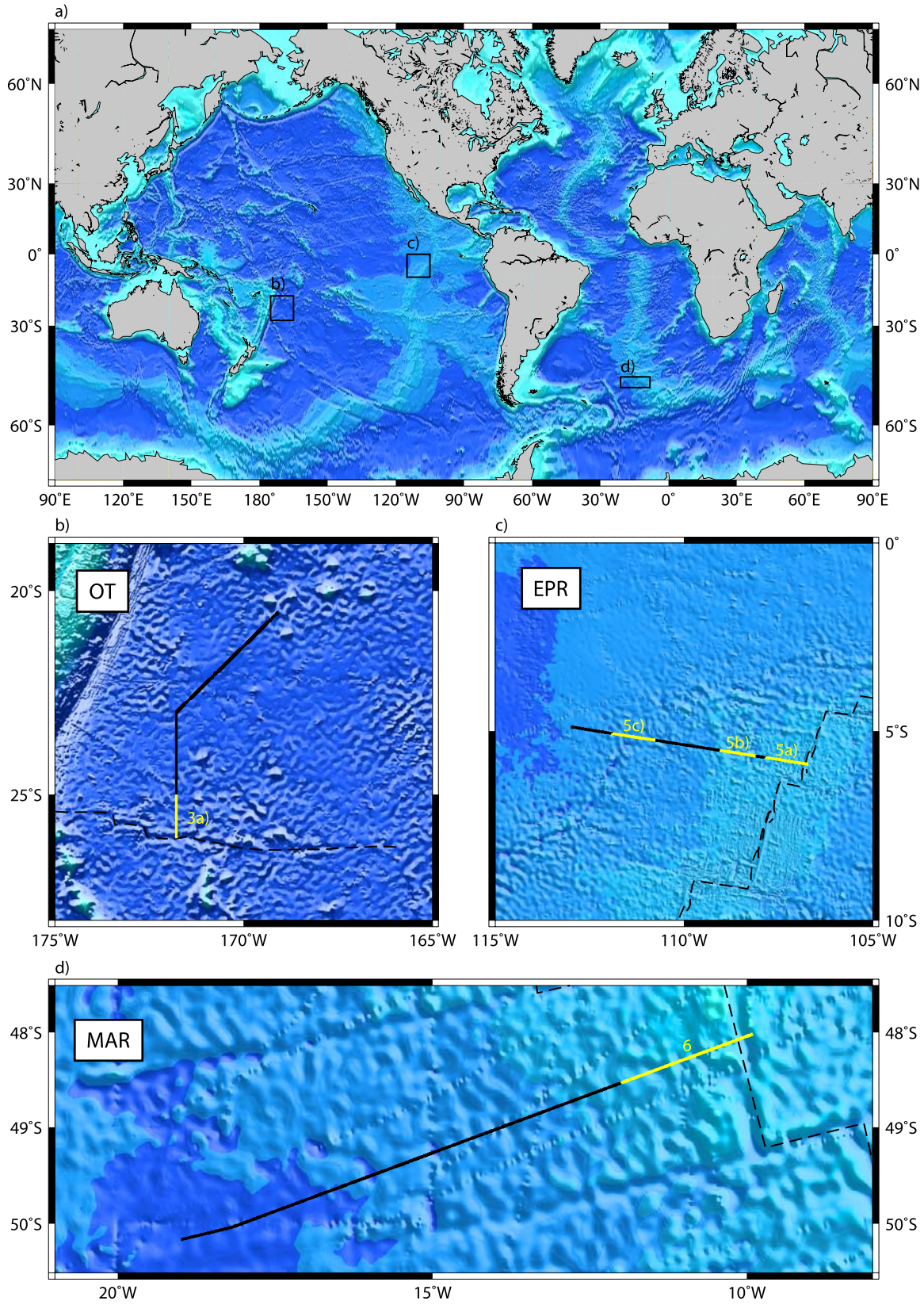
a)
60°N
30°N
0°
30°S
60°S
90°E
120°E
150°E
180°
150°W
120°W
90°W
60°W
30°W
0°
30°E
60°E
90°E
b)
c)
d)
b)
OT
20°S
25°S
175°W
170°W
165°W
3a)
c)
EPR
0°
5°S
10°S
115°W
110°W
105°W
5c)
5b)
5a)
d)
MAR
48°S
49°S
50°S
20°W
15°W
10°W
6

Figure 1

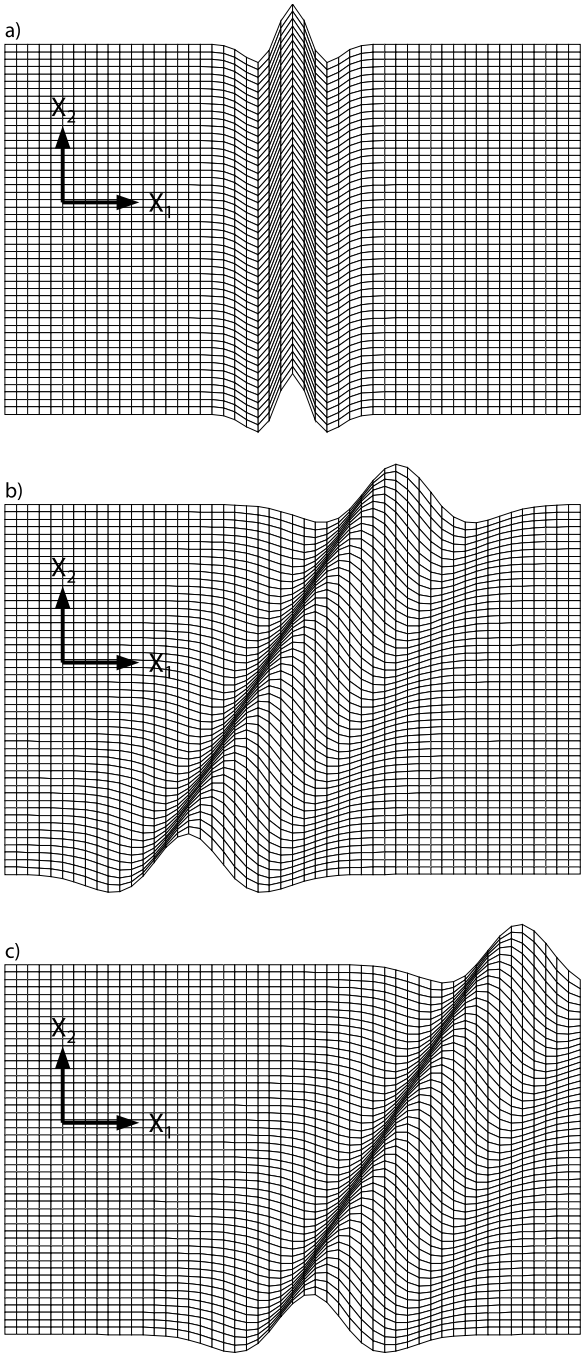

Figure 2. Example ridgelets similar to those used in our analysis. These functions are constant along one dimension and shaped like a Mexican Hat wavelet perpendicular to that dimension. Arrows indicate the directions of the x_1 and x_2 axes. θ is measured positive clockwise from x_2. (a) Reference ridgelet: $\theta = 0$, $a = a_o$, $b = b_o$. (b) Rotated and scaled version of Figure 2a: $\theta = 20°$, $a = 2a_o$, $b = b_o$. (c) Translated version of Figure 2b: $\theta = 20°$, $a = 2a_o$, $b > b_o$.

thermal swell could be analyzed separately from the small-scale features associated with the abandoned spreading center.

[7] *Little* [1994] and *Little and Smith* [1996] extended this technique to the analysis of 2-D SeaBeam data. For this analysis they created a 2-D analyzing function capable of enhancing abyssal hills of an a priori preferred orientation. These functions were applied to data collected near the Mid-Atlantic Ridge, and by selectively enhancing features oriented parallel to the ridge axis, were able to recreate an interpretation of abyssal-hill fabric made by identifying abyssal hills manually [*Little and Smith*, 1996].

[8] Our ridgelet transform method differs from that of *Little* [1994] and *Little and Smith* [1996] because it automatically determines abyssal-hill azimuths and scales for individual abyssal hills. These individual estimates are then averaged in regional groups such that populations of hills with statistically different properties are identified.

2.2. Definition of the Ridgelet Transform

[9] The ridgelet transform maps a function in a 2-D space-space domain to a 3-D space-azimuth-scale domain. It is defined as follows [*Candès and Donoho*, 1999; *Starck et al.*, 2003]. Choose a function, ψ: $\mathbb{R} \rightarrow \mathbb{R}$ (where $\mathbb{R}$ indicates the set of real numbers), with sufficient decay and which satisfies the wavelet definition [*Mallat*, 1998]:

$$\int \psi(s)ds = 0 \tag{1}$$

The corresponding ridgelet is defined for a scale parameter $a > 0$, a location parameter (we use along-track distance) $b \in \mathbb{R}$, and an azimuth parameter $\theta \in [0°, 360°)$ measured positive clockwise from the x_2 (northward) direction, as the function $\psi_{a,b,\theta}$: $\mathbb{R}^2 \rightarrow \mathbb{R}$ [*Candès and Donoho*, 1999]:

$$\psi_{a,b,\theta}(x_1, x_2) = \frac{1}{\sqrt{a}}\psi\left(\frac{x_1 \sin(\theta) + x_2 \cos(\theta) - b}{a}\right) \tag{2}$$

A plot of this function for various values of a, b and θ is presented in Figure 2. The ridgelet transform is given by.

$$R_f(a, b, \theta) = \int\int \overline{\psi}_{a,b,\theta}(x_1, x_2) f(x_1, x_2) dx_1 dx_2 \tag{3}$$

where f: $\mathbb{R}^2 \rightarrow \mathbb{R}$ is the function we wish to analyze.

[10] A ridgelet can be thought of as an infinitely anisotropic two-dimensional wavelet: it is constant

along the θ direction and has a cross-sectional shape given by dilations of ψ. When used in a ridgelet transform, the ridgelet function locates and characterizes the elongate features of f, similar to the anisotropic wavelets of *Gaillot et al.* [1999] and *Ouillon* [1996] and to the analyzing functions of *Little* [1994].

2.3. Digital Implementation of the Ridgelet Transform

[11] A useful property of the ridgelet transform is its relation to the Radon transform [*Bracewell*, 2000]. The Radon transform of a function f: $\mathbb{R}^2 \rightarrow \mathbb{R}$ is given by

$$Ra_f(\theta, s) = \int \int f(x_1, x_2)\delta(x_1, \sin(\theta) + x_2 \cos(\theta) - s)dx_1 dx_2 \tag{4}$$

where s is a location parameter (usually chosen to be one spatial dimension of the original signal) and θ is defined as before. The Radon transform maps a function from a space-space domain to a space-azimuth domain. If we use the one-dimensional wavelet transform along the space dimension of the Radon transform formula:

$$\int Ra_f(\theta, s)\psi_{a,b}(s)ds \tag{5}$$

where $\psi_{a,b}(s)$ is the dilated and translated wavelet:

$$\psi_{a,b}(s) = \frac{1}{\sqrt{a}}\psi\left(\frac{s-b}{a}\right) \tag{6}$$

with a and b defined as before, we recover the ridgelet transform (equation (3)).

[12] This property suggests a method by which we can calculate the ridgelet transform of a data set: first transform to the Radon domain, then apply a 1-D wavelet transform along lines of constant θ [*Starck et al.*, 2002, 2003].

[13] The 2-D ridgelet transform maps linear features in a two-dimensional space-space domain to maxima in a three-dimensional location-scale-azimuth domain. By applying the ridgelet transform, with appropriate ψ, to multibeam bathymetry and then locating maxima in the ridgelet domain we are able to determine the dominant scale and azimuth of abyssal ridges along a multibeam swath. It is therefore relatively simple to detect the location and scale of systematic changes in these parameters using statistical tests. The local RMS amplitude is easily calculated during our implementation of the ridgelet transform (see section 3.1).

[14] The ridgelet transform is invertible [*Starck et al.*, 2002, 2003]; however, invertibility is not necessary for our analysis because we interpret our data directly in the ridgelet domain. This ridgelet domain analysis allows us considerable latitude in the design and implementation of the ridgelet transform algorithm. We first Radon transform the bathymetry data by numerically calculating the line integrals given by equation (4) in the spatial domain. Because multibeam data are collected in swaths, a bias is introduced when calculating the Radon transform, i.e., along-track azimuths will have a longer domain of integration in (4) than will cross-track azimuths. A space-domain implementation allows us to avoid this bias by restricting the length of the along-track Radon integrals. A space-domain calculation also allows us to normalize the Radon integral (4) by the length of the line along which the data are summed, avoiding the problem of irregular edges and gaps in the data. This normalization yields an "average" bathymetry along an azimuth, allowing for a more physical interpretation of the Radon-transformed data. This Radon transform process also results in a regular gridding of the data in the Radon domain allowing us to use standard Fast Fourier Transform techniques to calculate the wavelet transform during the transformation of the data to the ridgelet domain.

3. Application of the Ridgelet Transform to Abyssal-Hill Morphology

3.1. Example Ridgelet Transform of Multibeam Data

[15] We use a section of multibeam data collected north of the Osbourn Trough [*Lonsdale*, 1997] by the research-vessel icebreaker (R/VIB) *Nathaniel B. Palmer* during cruise NBP0304 in 2003 (Figure 1) to illustrate the ridgelet transform (Figure 3). The Osbourn Trough is located between 26°S and 26°15′S at the bottom of Figure 3a.

[16] Our Radon transform algorithm takes a gridded multibeam data set as input (we use a 200 m grid spacing) and a series of track points that (approximately) run down the center of the multibeam swath. The track points parameterize the "location" for the location-azimuth output of the Radon transform. For each track point we only use the data within a 10 km radius (the Radon aperture), which is approximately half the width of a multibeam swath. We calculate the average bathymetry of the data in that window and subtract

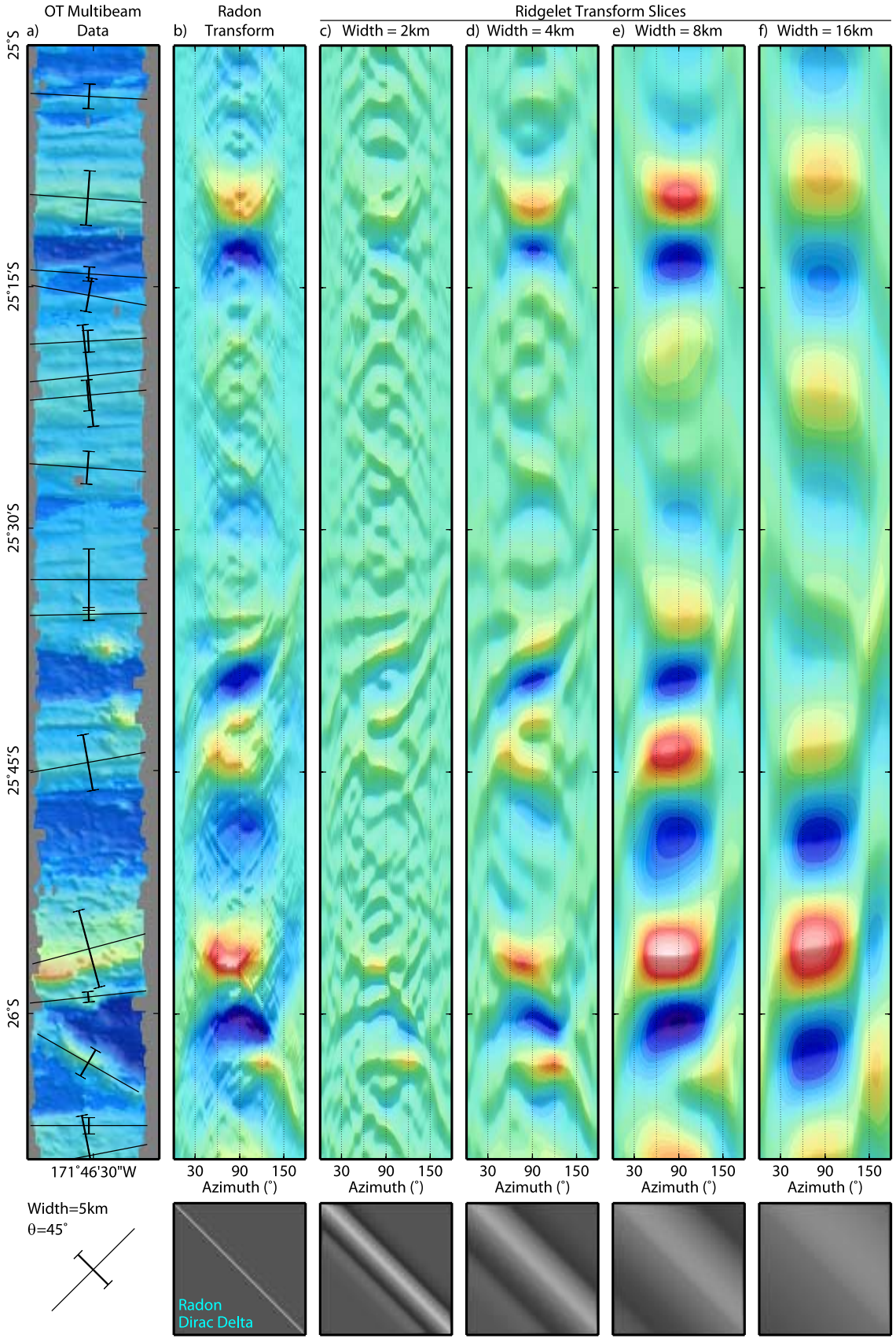
OT Multibeam
a) Data
Radon
b) Transform
Ridgelet Transform Slices
c) Width = 2km
d) Width = 4km
e) Width = 8km
f) Width = 16km
25°S
25°15'S
25°30'S
25°45'S
26°S
171°46'30"W
30 90 150
Azimuth (°)
Width=5km
θ=45°
Radon
Dirac Delta

Figure 3

it from the data within the window to yield a bathymetric anomaly. The RMS amplitude of this anomaly is our local measure of the RMS amplitude of the abyssal hills (we also simultaneously calculate the RMS amplitude of the bathymetry within a 20 km-radius window for comparison). The 10 km-radius window restricts our analysis to wavelengths less than ~20 km. A similar wavelength band was used by *Hayes and Kane* [1991] in their analysis of abyssal-hill RMS amplitude.

[17] Next, the Radon integral (4) is calculated along lines intersecting the track point with azimuths varying from 0° to 180°. The result of these integrals for each azimuth is then normalized by the length of the integral through regions of defined bathymetry (i.e., the Radon integral is not calculated over gaps in the data). The final output, after this process has been applied to all track points, is the Radon transform of the bathymetric anomaly in a track point-azimuth domain. The output of our Radon transform algorithm for the example data set is shown in Figure 3b.

[18] Features localized near a single point of the spatial domain become localized along lines in the Radon domain. In a location-azimuth space these lines follow the shape of the tangent function. This effect can be seen by examining the Radon transform of the two seamounts near 25°37′S (Figure 3a). These seamounts appear in Figure 3b as low-amplitude linear anomalies in the shape of tangent curves centered at 90°. Conversely the Radon transform concentrates linear features in the spatial domain at single points of the Radon domain. The location of these points coincides with the azimuth and location of their parent features in the spatial domain. There is a small NW–SE trending ridge located within the Osbourn Trough at 26°4′S in Figure 3a. This ridge maps to a peak in the Radon domain at 120° azimuth (Figure 3b). The peaks in Figure 3b corresponding to narrow ridges on the seafloor are much more localized than are the peaks corresponding to wide abyssal ridges. For narrow abyssal ridges, a small range of azimuths lay along the top of the abyssal ridges (i.e., the region where the abyssal ridge is significantly higher than the abyssal plain). However, for wider abyssal ridges, the range of azimuths that lay along the region of high bathymetry is much larger. Therefore the width of a peak in the Radon domain is wider in azimuth for large-scale abyssal hills than for small-scale abyssal hills. This effect is reduced by increasing the width of the multibeam swath by combining data from two adjacent swaths and using a correspondingly larger Radon aperture.

[19] Because the Radon transform resolution depends on abyssal-hill scale, a further separation of the data based on scale is desired. This separation is accomplished during the second step of the ridgelet transform. The wavelet that we choose to use for this step is the Mexican Hat wavelet (Figure 4), which is defined as the second derivative of a Gaussian:

$$\psi(x) = -\frac{d^2}{dx^2} e^{-\left(x^2/2\right)} = \left(1 - x^2\right) e^{-\left(x^2/2\right)} \tag{7}$$

The Mexican Hat wavelet satisfies the following equation, when $\Gamma = \mathbb{R}$:

$$\int_{\Gamma} \psi(x) x^n dx = 0, n = 0, 1 \tag{8}$$

[20] For $n = 0$, this equation reduces to the wavelet definition (1) and the $n = 1$ case demonstrates that the Mexican Hat wavelet has zero linear moment. Because the Mexican Hat wavelet is localized to a small region of $\mathbb{R}$, called its "effective support"

Figure 3. (a) Example data set consisting of a section of the NBP0304 multibeam data north of the Osbourn Trough. This data set contains two prominent seamounts near 25°37′S, numerous abyssal-hills and a single ridge contained within the axis of the Osbourn Trough at 26°6′S. (b) Radon transform of the data set in Figure 3a. The seamounts appear as tangent function shaped features. Most of the abyssal-hills show up as maxima near 90°. However, the ridge in the trough axis strikes at 120° and appears in Figure 3b as a maximum at the location appropriate to that azimuth. Note that the smallest ridges in Figure 3a form well-localized maxima in Figure 3b, relative to the maxima of larger ridges. This difference in behavior between scales leads naturally to the multiscale decomposition of these data presented in Figures 3c–3f. The box beneath Figure 3b shows a schematic of the Dirac ridge used in the Radon transform to analyze the data in Figure 3a. Figures 3c–3f present a particular slice through the ridgelet transform at the width indicated. A sample ridgelet corresponding to each width is plotted in the box beneath each panel at the scale of the data in Figure 3a. The resolution in azimuth is best for the smallest-scale abyssal hills. The location of the maxima in these slices gives a measure of the location and azimuth of a particular abyssal hill. The width at which each abyssal-hill maxima has largest amplitude is the measure of the width of that abyssal hill. The locations, azimuths, and widths of each maxima in the ridgelet domain are plotted in Figure 3a with a symbol consisting of a line segment parallel to the azimuth, and a superimposed I-shaped symbol at 90 degrees to the azimuth whose length equals the width location of each maxima. A sample symbol for a northeast trending 5 km wide hill is shown beneath Figure 3a.

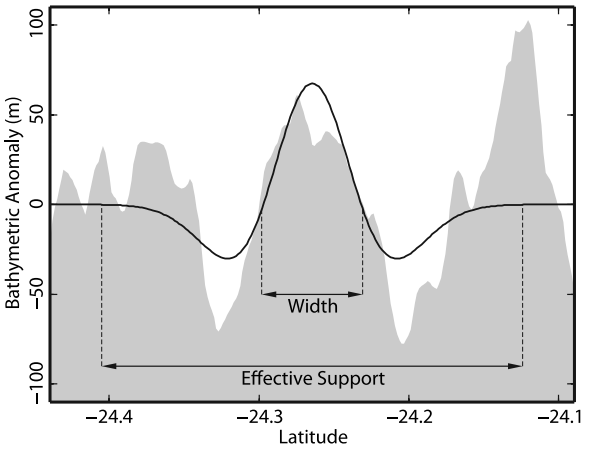

Figure 4. Example Mexican Hat wavelet superimposed on the Radon transform of the NBP0304 data at $\theta = 90°$ and the latitudes shown. The scale and translation of the wavelet match a peak in the ridgelet transform of the data. The width of the wavelet is defined as the distance between zero-crossings of the wavelet. Note also that the wavelet is effectively zero outside the region of its "effective support."

(see Figure 4), equation (8) holds approximately when Γ is equal to the effective support. The Mexican Hat wavelet is insensitive to the mean and any linear trend in the data over the wavelet's effective support, so we are able to measure the scales of small ridges superimposed on large ridges independently, as the large ridge is approximately linear at the scale of the smaller ridge. Also, because the Mexican Hat wavelet is symmetric, peaks in the Radon domain correspond to peaks in the ridgelet domain, preserving their sign. Thus local minima in the ridgelet domain correspond to trenches and local maxima correspond to ridges. The locations of the maxima in the ridgelet domain provide us with a local measure of the azimuth and scale of abyssal hills.

[21] The wavelet transform increases the dimensionality of the data by one, taking us from the 2-D azimuth-location domain of the Radon transformed data to the 3-D azimuth-location-scale domain of the ridgelet transformed data. To compare our results with those of previous studies it is necessary to convert the scale, which is a relative measure of wavelet size, to a width parameter expressed in kilometers. We define this new width parameter to be the distance between the zero crossings of the Mexican Hat wavelet of appropriate scale (Figure 4).

[22] Figures 3c–3f show the output of the ridgelet transform of the data in Figure 3a as several constant-width slices through the ridgelet transform output. Because the Radon transform utilizes a "Dirac ridge" (see the square panel below Figure 3b) to transform data, it is sensitive to all linear features in the data regardless of the scale (width) of those features. A ridgelet corresponding to the widths of the slices in Figures 3c–3f are plotted, at the scale of the data in Figure 3a, in the square panel beneath each slice. These ridgelets are only sensitive to linear features in the data that have a width close to that of the ridgelet itself. Described in this way, the ridgelet transform of the data for a specified scale can be interpreted as a band-limited Radon transform. Thus Figures 3c–3f can be thought of as a scale decomposition of Figure 3b.

[23] As noted above, the peaks corresponding to the small-scale ridges in the space domain are much smaller in azimuth than the peaks corresponding to large-scale ridges. The azimuth resolution is constant across each ridgelet slice; therefore the ridgelet transform also separates the well-resolved small-scale features from the poorly resolved large-scale ones. Increasing the size of the Radon aperture would help to better resolve the large-scale features. In this case, however, the size of the Radon aperture is limited to the width of the multibeam swath. A wider swath width (or 2 swaths next to each other) would improve the resolution in azimuth at our scales of interest. For a constant azimuth, the ridgelet transform has the same resolution characteristics as the wavelet transform: better location resolution at small scales and better scale resolution at large scales [*Mallat*, 1998].

[24] By examining Figures 3c–3f we can see that the peak corresponding to the small ridge at 26°4′S has highest amplitude for a width of 4 km. We can therefore estimate this abyssal hill's width as 4 km and its azimuth as 120°. Similarly the ridge bounding the northern side of the Osbourn Trough at 25°56′S has a dominant width of 8 km and an azimuth of ~80°. On Figure 3a, we have marked the azimuth and scale at the appropriate location for each ridgelet maxima by a symbol consisting of a line segment that parallels the ridge axis, and an I-shaped symbol oriented 90° to the line segment, whose length equals the width of each ridge. A sample symbol for an azimuth of 45°and a width of 5 km is shown beneath Figure 3a.

3.2. Results of Ridgelet Analysis of the Osbourn Trough, East Pacific Rise, and Mid-Atlantic Ridge Data Sets

[25] In addition to the Osbourn Trough multibeam data, we also applied our ridgelet transform method

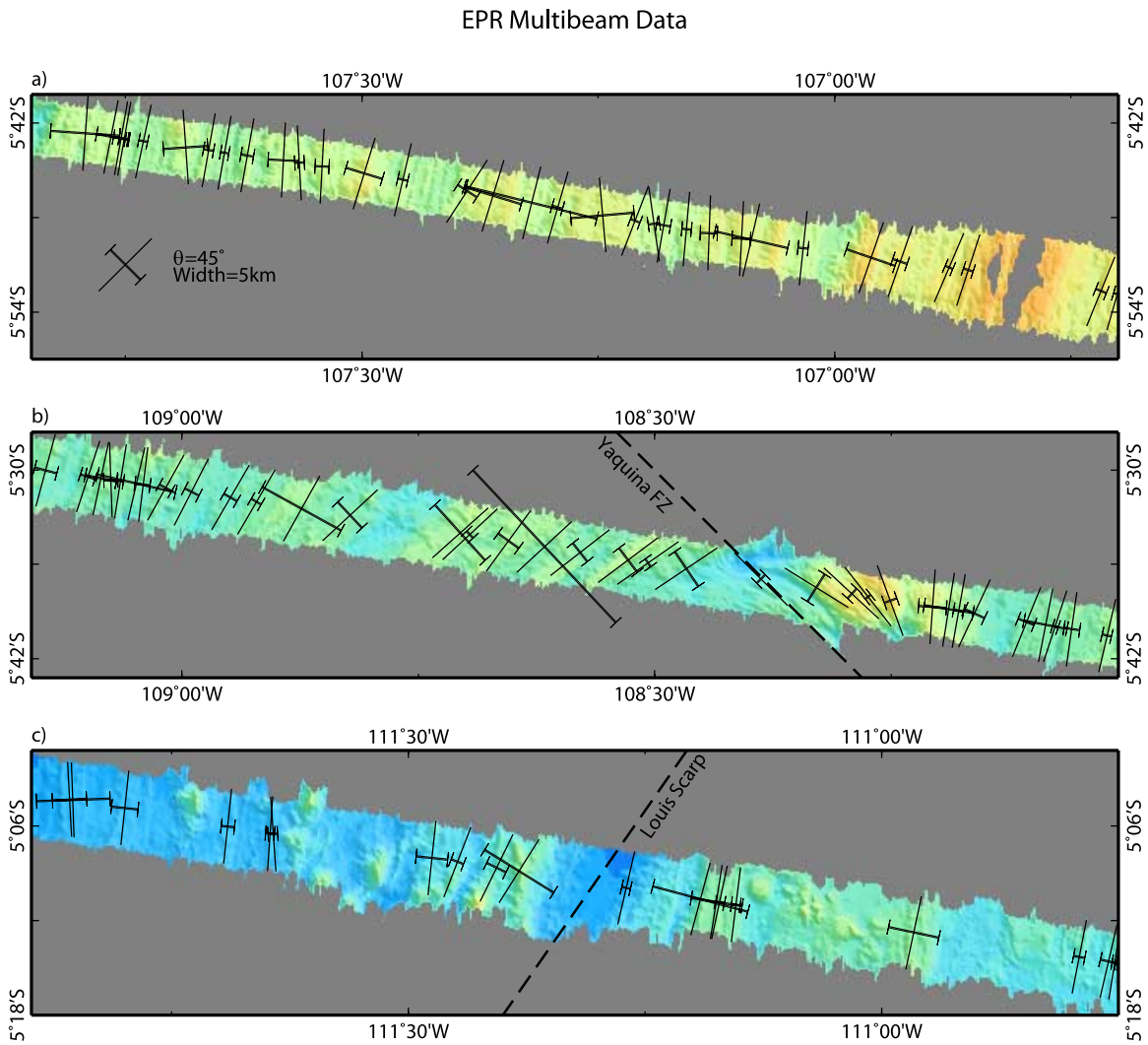

Figure 5. (a) A sample of the EPR multibeam swath. The East Pacific Rise is located at 106°42′W in this figure. The location of each ridgelet maxima is plotted using the same symbol used in Figure 3a. (b) Same as Figure 5a but for the anomalous region of seafloor fabric observed near the Yaquina Fracture Zone (FZ). (c) Detail of the anomalous multibeam data collected near the Louis Scarp.

to two other multibeam swaths (Figure 1). The East Pacific Rise (EPR) data set was acquired by the R/V *Revelle* in 1997 (cruise GENE04), while the Mid-Atlantic Ridge (MAR) data set was acquired onboard the R/V *Melville* in 2002 (cruise VANC05). A sample of the output of our ridgelet transform analysis of these additional swaths is shown in Figures 5 and 6. The East Pacific Rise is located at longitude 108°48′W in Figure 5a, and the Mid-Atlantic Ridge is located near 10°3′W in Figure 6. The widths and azimuths of the abyssal hills are marked in Figures 5 and 6 using the same scheme as in Figure 3a. The three data sets presented here were chosen because they were collected during transits across a spreading center (or extinct spreading center in the case of the Osbourn Trough) and therefore are long stretches of a single swath. Furthermore these swaths survey bathymetry created at much different spreading rates. The EPR data set surveys crust created at roughly 14 cm/yr [*Small*, 1998] whereas the MAR data set surveys crust created at 3.3 cm/yr [*DeMets et al.*, 1990]. The paleo-spreading rate of the Osbourn spreading center is estimated to have been 6–8 cm/yr [*Billen and Stock*, 2000].

[26] The output of the application of our ridgelet transform procedure to the multibeam data acquired during all three cruises is shown in Figures 7–9 and Table 1. Figure 7 displays the results of the ridgelet analysis of the EPR data set. This data set includes two regions of anomalous

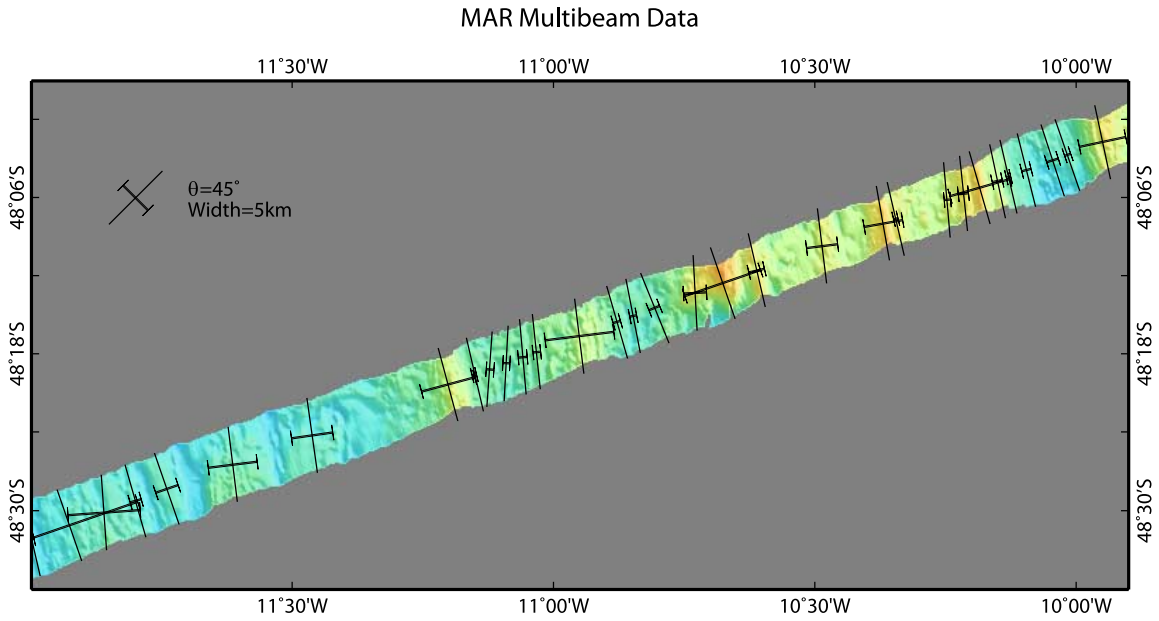

Figure 6. A sample of the MAR multibeam swath. The Mid-Atlantic Ridge is located at 10°3′W in this figure.

abyssal-hill shape. The eastern anomalous region extends from 109°3′W to 108°12′W (Figure 5b) and is characterized by an increased RMS amplitude and NE and NW trending abyssal hills, values much different from the regional abyssal-hill trends (see Figures 7a and 7c). The location of this anomalous region coincides with the trace of the Yaquina Fracture Zone (Figure 5b) as mapped by *Eakins and Lonsdale* [2003]. The western region of anomalous bathymetry extends from 111°54′W to 110°45′W (Figure 5c) and is likewise characterized by increased RMS amplitude, but does not exhibit any unusual abyssal-hill trends. This corresponds to the location of the Louis Scarp [*Eakins and Lonsdale*, 2003]. These two anomalous regions provide natural boundaries between regions of relatively constant abyssal-hill properties. Therefore we divide the EPR abyssal hills into three populations (Figure 6). Group EPR 1 consists of abyssal hills observed west of the Louis Scarp, EPR 2 contains those observed between the Louis Scarp and the Yaquina Fracture Zone and EPR 3 are the abyssal hills observed east of the Yaquina Fracture Zone. All three populations exhibit similar RMS amplitudes, ranging from 50–100 m, a range typical of crust created at fast spreading centers [*Goff et al.*, 1997]. Similarly, all three populations exhibit a similar mean abyssal-hill width. However, these widths vary widely in all three populations. The Louis Scarp, however, marks the location of a change in abyssal-hill strike. Population EPR 1 has a mean azimuth of 5.1° and an angular deviation [*Cain*, 1989] of 8.6°, while EPR 2 has mean azimuth of 12.3 ° and angular deviation of 7.3° (Table 1). The result of a Watson-Williams test [*Zar*, 1999] shows that these means are significantly different with 95% confidence. Thus the Louis Scarp may mark the location of a change in spreading direction.

[27] The results of the ridgelet analysis of the MAR data set are shown in Figure 8. Unlike the EPR abyssal hills, the azimuths of the MAR abyssal hills do not vary significantly along the ship track, and we see no reason to separate these abyssal hills into separate populations on the basis of their shapes and locations. The widths also vary widely, with a slightly higher mean value than the EPR abyssal hills, as would be expected for slower spreading centers; however, the large scatter of widths makes it impossible to determine if this difference is significant. The RMS amplitude of the bathymetry near the Mid-Atlantic Ridge is in general much larger than that of the EPR, ranging from 100–400 m, a range that is in agreement with that of typical slow-spreading regions [*Goff et al.*, 1997]. However, farther from the Mid-Atlantic Ridge, RMS amplitudes decrease markedly. This decrease in seafloor roughness is most likely due to an increase in sediment cover (gray line in Figure 7c) which artificially smoothes seafloor bathymetry.

[28] There is a change in abyssal-hill azimuth for the Osbourn Trough data set (Figure 8) at approx-

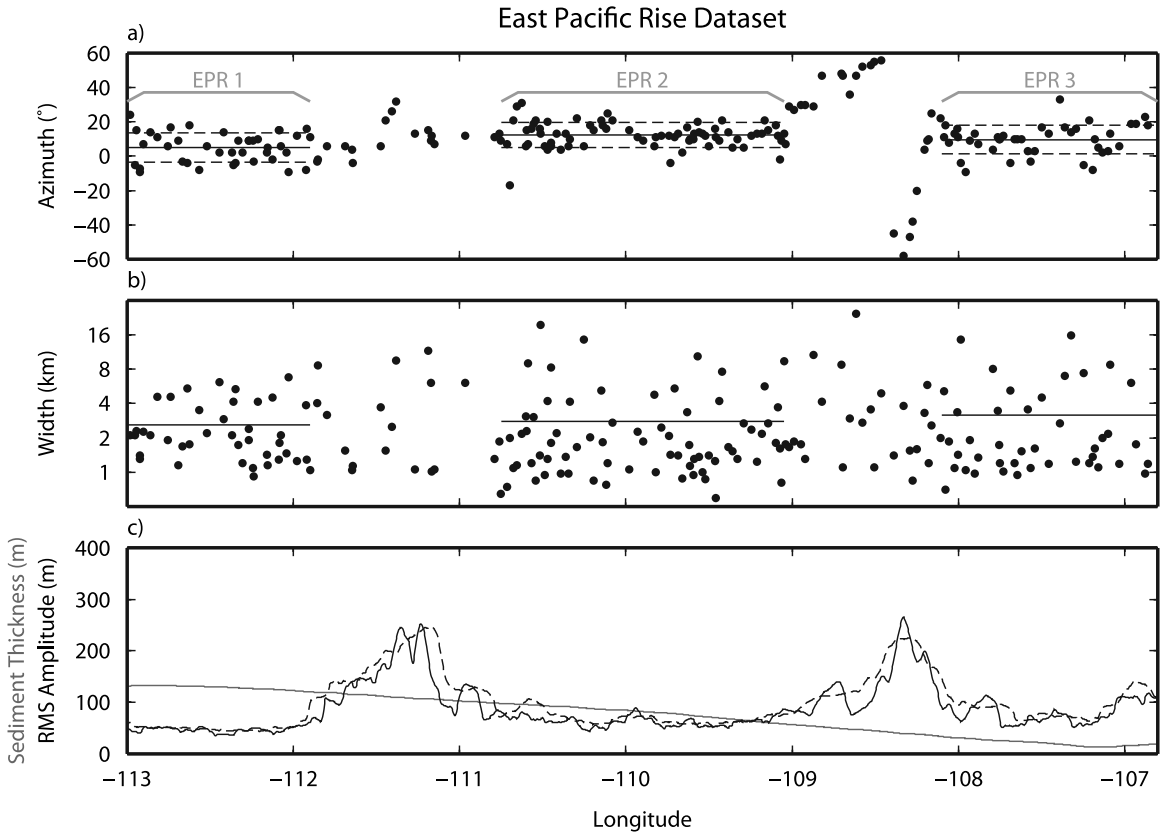

Figure 7. Output of the ridgelet transform method for the EPR multibeam data. The Louis Scarp and Yaquina Fracture Zone provide natural boundaries between three populations of abyssal hills, which we denote as EPR 1, 2, and 3. (a) Azimuths of the observed abyssal hills. The gray lines denote the locations of the EPR 1, 2, and 3 populations. For each population, the mean azimuth is plotted as a solid line, and the mean ± one angular deviation [*Cain*, 1989] are plotted as two dotted lines. The azimuth of the EPR abyssal hills changes across the Louis Scarp, from 5.1° for EPR 1 west of the scarp to 12.3° for EPR 2 east of the scarp, a difference that is statistically significant. With the exception of a few anomalous abyssal hills near the Yaquina Fracture Zone, the azimuth of abyssal hills does not significantly change east of the Louis Scarp, with a mean of 9.7° for the EPR 3 abyssal hills. (b) The widths of these abyssal hills vary widely, and no clear trend or change in abyssal-hill widths is observed between the three populations. The mean width of each population is plotted as a solid line. (c) RMS amplitude of the EPR bathymetry, calculated using a 10-km-radius (solid black line) and a 20-km-radius (dashed black line) window. Also plotted is the sediment thickness along the multibeam swath taken from the NGDC global sediment database [*Divins*, 2006]. The RMS amplitude is within the range of 50–100 m for all three groups of abyssal hills, a value typical of fast spreading ridges. The RMS amplitude of bathymetry increases markedly near the locations of the Louis Scarp and Yaquina Fracture Zone.

imately 23°S. Abyssal hills between 20°S and 22°S (group OT 1) have mean trend of 98.3° and an angular deviation of 7.1° while abyssal-hills between 24°S and 26°S (group OT 3) have mean trend 90.6° and an angular deviation of 6.8°. The result of a Watson-Williams test shows that these two populations have different means at a 95% confidence level. However, the abyssal hills between 22°S and 24°S (group OT 2) have a mean trend of 93.9° which is not significantly different from the means of either groups OT 1 or OT 3. Unlike the relatively sudden shifts of abyssal-hill azimuths observed at the Louis Scarp, this change in azimuth appears to occur over a larger scale. Two possible geologic scenarios which would result in a change in abyssal-hill trend are a change in paleo-spreading direction along this multibeam swath, or the presence of a triple junction trace between 22°S and 24°S. The widths of the OT abyssal hills are typically about 5 km. The sediment thickness along the OT data set is in general quite thin, so sediment smoothing should not affect our estimates of seafloor roughness there. The RMS amplitudes of this data set are also quite low, near 50–100 m, with the exception of the region immediately north of the Osbourn Trough which exhibits

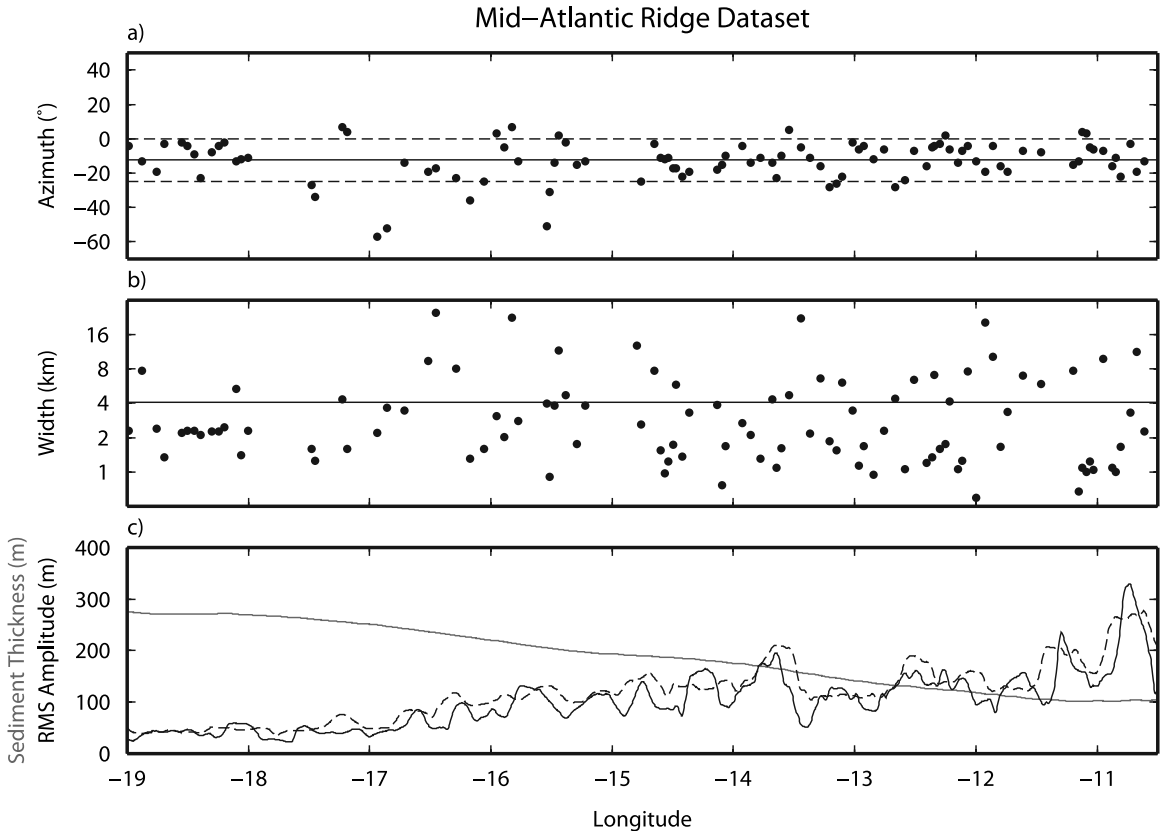

Figure 8. Output of the ridgelet transform algorithm for the MAR multibeam data. Unlike the EPR abyssal hills, there are no clear boundaries observed in the data. (a) The azimuths of MAR abyssal hills remain relatively constant across the survey area, with a mean value of −12.5° (solid line) and an angular deviation of 12.4° (dotted lines). (b) The widths are also scattered similar to those of the EPR abyssal hills, with a slightly higher mean width of 4.1 km (solid line). (c) The RMS amplitude near the MAR axis, which is typical of slow spreading rates. The RMS amplitude decreases steadily with increasing distance to the MAR. This decrease in smoothness is correlated with sediment thickness, which increases with distance from the ridge. The decrease in RMS amplitude therefore is attributed to the smoothing effect of thick sediment cover.

roughness of 50–300 m. This pattern of roughness of the Osbourn Trough data set may result from a significant slowing of spreading rate prior to the extinction of the Osbourn Trough.

4. Discussion and Conclusions

[29] Our ridgelet transform method is capable of locally estimating abyssal-hill width, azimuth and RMS amplitude. It should also be possible to modify our method to quantify other aspects of abyssal-hill shape. Using asymmetric wavelets in conjunction with the Mexican Hat wavelet utilized here may quantify abyssal-hill asymmetry using the ridgelet transform. The estimation of abyssal-hill shape should be especially useful for studies of regions where other data types are unavailable for constraining tectonic models, such as regions created during periods of constant magnetic polarity.

[30] A particularly important aspect of our method is that it simplifies detecting changes in abyssal-hill shape, which is a possible indicator of a change in spreading rate or direction. We are able to use our method to detect a change in spreading direction at the Louis Scarp west of the EPR, a possible change in spreading direction, or the location of a triple junction trace, north of the Osbourn Trough, and a possible decrease in spreading rate prior to the extinction of the Osbourn paleo-spreading center. Determining when any change in spreading direction or rate occurred, however, is not directly possible using multibeam data. Unlike magnetic reversal data there is no timescale associated with changes in abyssal-hill morphology. Other data,

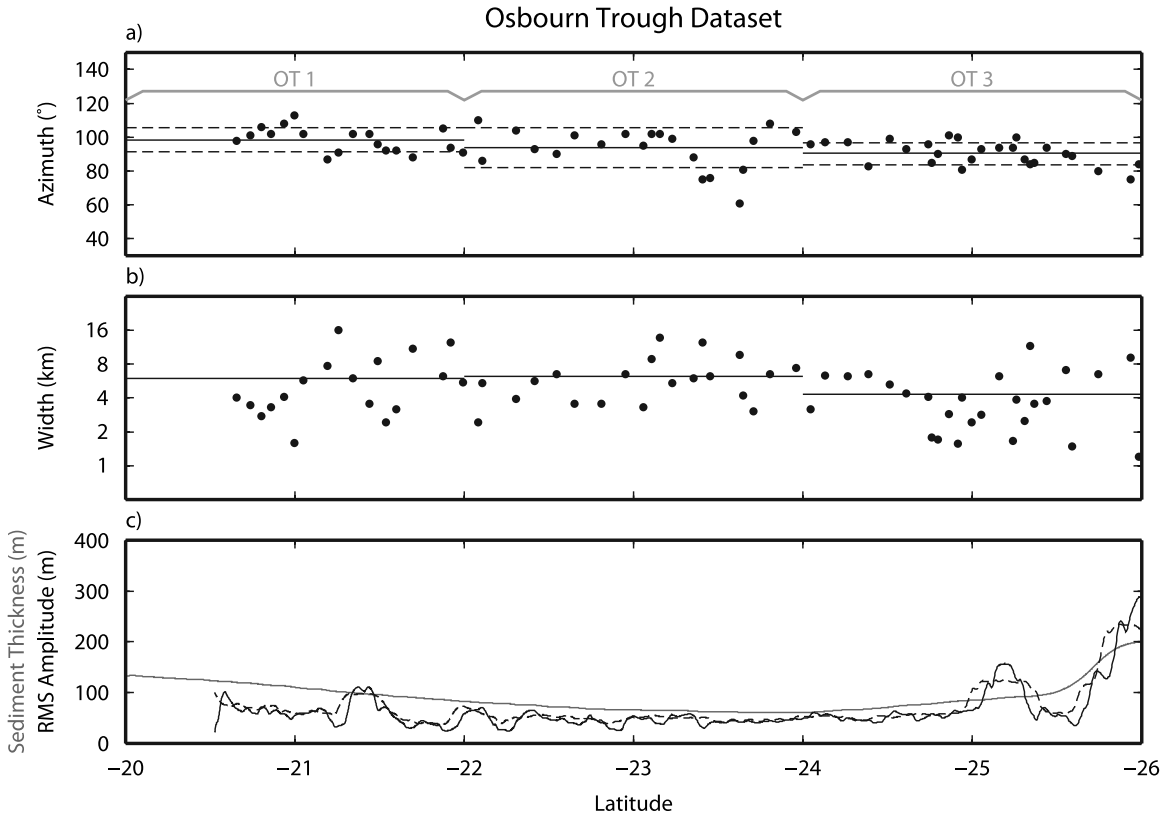

Figure 9. Output of the ridgelet transform algorithm for the OT multibeam data. (a) The abyssal-hills in this figure have been separated into three groups, based on latitude, as shown by the gray lines. Group OT 1 has mean trend 98.3°, group OT 2 has mean trend 93.9°, and group OT 3 has mean trend 90.6°. Watson-Williams tests [*Zar*, 1999] show that groups OT 1 and OT 3 have significantly different means; however, group OT 2's mean is not significantly different from either group OT 1 or OT 3. This change in abyssal-hill trend may be evidence of either a change in the spreading direction of the Osbourn paleo-spreading center or the presence of a triple junction trace between 22°S and 24°S. Unlike the relatively sudden change in abyssal-hill trend at the Louis Scarp, this transition in trend occurs over a larger scale. (b) Widths of abyssal hills near the Osbourn Trough. There are no significant trends across the survey area. (c) The RMS amplitude of abyssal hills along the survey. The amplitude is highest near the Osbourn Trough axis and may indicate a change in spreading rate prior to extinction of the Osbourn paleo-spreading center.

such as radiometric dating of dredge or core samples, are required to fully constrain the tectonic history of a region via abyssal-hill morphology.

[31] There are several potential sources of error in our ridgelet analysis. Any process that modifies the shape of abyssal hills after their formation will affect the results of any bathymetry analysis. Two of the most prevalent processes are intraplate volcanism resulting in the formation of seamounts and the modification of seafloor shape by sedimen-

Table 1. Abyssal Hill Population Statistics

Population	Mean Azimuth, deg	Angular Deviation, deg	Mean Width, km	Width Standard Deviation, km
EPR 1	5.1	8.6	2.6	1.6
EPR 2	12.3	7.3	2.8	3.2
EPR 3	9.7	8.5	3.2	3.5
MAR	−12.5	12.4	4.1	4.6
OT 1	98.3	7.1	6.0	3.8
OT 2	93.9	11.9	6.2	3.0
OT 3	90.6	6.8	4.3	2.6

tation. Small point features in the multibeam data are sufficiently averaged out during the Radon transform, but large seamounts can affect the output if their height exceeds the amplitude summed along nearby abyssal ridges.

[32] In the regions where abyssal-hill analysis may be most useful for tectonic reconstructions (i.e., those created during the Cretaceous Long Normal Polarity Interval; Chron C34, 83–121 Ma [*Cande and Kent*, 1995]) sediment cover can be relatively thick. Sediment cover tends to smooth out bathymetry by reducing the RMS amplitude and damping the expression of small-scale features. Therefore it is important to know the sediment thickness near multibeam surveys. Seismic data and drilling may provide some control on sediment thickness. Ultimately, however, the errors that may affect the results of our ridgelet transform method must be examined on a region by region basis.

Acknowledgments

[33] NBP0304 was supported by NSF grant OPP-0126334. Subsequent data analysis was supported by NSF grant OPP-0338317. We thank John Goff and an anonymous reviewer for their thorough and insightful reviews of the manuscript. We also thank J. Stock, S. Cande, and N. Smith-Downey for useful comments. California Institute of Technology Division of Geological and Planetary Sciences, contribution 9153.

References

Billen, M., and J. Stock (2000), Morphology and origin of the Osbourn Trough, *J. Geophys. Res.*, *105*, 13,481–13,489.

Bracewell, R. (2000), *The Fourier Transform and Its Applications*, McGraw-Hill, New York.

Buck, W., and A. Polikov (1998), Abyssal hills formed by stretching oceanic lithosphere, *Nature*, *392*, 272–275.

Cain, M. (1989), The analysis of angular data in ecological field studies, *Ecology*, *70*, 1540–1543.

Cande, S. C., and D. V. Kent (1995), Revised calibration of the geomagnetic polarity timescale for the Late Cretaceous and Cenozoic, *J. Geophys. Res.*, *100*(B4), 6093–6096.

Candès, E. (1998), Ridgelets: Theory and application, Ph. D. thesis, 116 pp., Stanford Univ., Stanford, Calif.

Candès, E., and D. Donoho (1999), Ridgelets: A key to higher-dimensional intermittency?, *Philos. Trans. R. Soc. London, Ser. A*, *357*, 2495.

DeMets, C., A. Gordon, D. Argus, and S. Stein (1990), Current plate motions, *Geophys. J. Int.*, *101*, 425–478.

Divins, D. L. (2006), Total sediment thickness of the world's oceans and marginal seas, Natl. Geophys. Data Cent., Boulder, Colo. (Available at http://www.ngdc.noaa.gov/mgg/sedthick/sedthick.html)

Eakins, B., and P. Lonsdale (2003), Structural patterns and tectonic history of the Bauer microplate, Eastern Tropical Pacific, *Mar. Geophys. Res.*, *24*, 171–205.

Gaillot, P., J. Darrozes, and J. Bouchez (1999), Wavelet transform: A future of rock fabric analysis?, *J. Struct. Geol.*, *21*, 1615–1621.

Goff, J. (1991), A global and regional stochastic analysis of near-ridge abyssal hill morphology, *J. Geophys. Res.*, *96*, 21,713–21,737.

Goff, J., and T. H. Jordan (1988), Stochastic modeling of seafloor morphology: Inversion of Sea Beam data for second-order statistics, *J. Geophys. Res.*, *93*, 13,589–13,608.

Goff, J., B. Tucholke, J. Lin, G. Jaroslow, and M. Kleinrock (1995), Quantitative analysis of abyssal hills in the Atlantic Ocean: A correlation between inferred crustal thickness and extensional faulting, *J. Geophys. Res.*, *100*, 22,509–22,522.

Goff, J., Y. Ma, A. Shah, J. Cochran, and J. Sempere (1997), Stochastic analysis of seafloor morphology on the flank of the Southeast Indian Ridge: The influence of ridge morphology on the formation of abyssal hills, *J. Geophys. Res.*, *102*, 15,521–15,534.

Hayes, D., and K. Kane (1991), The dependence of seafloor roughness on spreading rate, *Geophys. Res. Lett.*, *18*, 1425–1428.

Kriner, K., R. Pockalny, and R. Larson (2006), Bathymetric gradients of lineated abyssal hills: Inferring seafloor spreading vectors and a new model for hills formed at ultra-fast rates, *Earth Planet. Sci. Lett.*, *242*, 98–110.

Kumar, P., and E. Foufoula-Georgiou (1997), Wavelet analysis for geophysical applications, *Rev. Geophys.*, *35*, 385–412.

Larson, R., R. Pockalny, R. Viso, E. Erba, L. Abrams, B. Luyendyk, J. Stock, and R. Clayton (2002), Mid-Cretaceous tectonic evolution of the Tongareva triple junction in the southwest Pacific Basin, *Geology*, *30*, 67–70.

Little, S. (1994), Wavelet analysis of seafloor bathymetry: An example, in *Wavelets in Geophysics*, edited by E. Foufoula-Georgiou and P. Kumar, pp. 167–182, Elsevier, New York.

Little, S., and D. Smith (1996), Fault scarp identification in side-scan sonar and bathymetry images from the Mid-Atlantic Ridge using wavelet-based digital filters, *Mar. Geophys. Res.*, *18*, 741–755.

Little, S., P. Carter, and D. Smith (1993), Wavelet analysis of a bathymetric profile reveals anomalous crust, *Geophys. Res. Lett.*, *20*, 1915–1918.

Lonsdale, P. (1997), An incomplete geologic history of the south–west Pacific basin, *Geol. Soc. Am. Abstr. Programs*, *29*, 4574.

Macdonald, K., R. Fox, R. Alexander, R. Pockalny, and P. Gente (1996), Volcanic growth faults and the origin of Pacific abyssal hills, *Nature*, *380*, 125–129.

Mallat, S. (1998), *A Wavelet Tour of Signal Processing*, 637 pp., Elsevier, New York.

Menard, H. W. (1967), Sea floor spreading, topography and the second layer, *Science*, *157*, 923–924.

Ouillion, G. (1996), Hierarchical geometry of faulting, *J. Geophys. Res.*, *101*, 5477–5487.

Small, C. (1998), Global systematics of mid-ocean ridge morphology, in *Faulting and Magmatism and Mid-Ocean Ridges*, *Geophys. Monogr. Ser.*, vol. 106, edited by Buck et al., pp. 1–25, AGU, Washington, D. C.

Starck, J., E. Candès, and D. Donoho (2002), The curvelet transform for image denoising, *IEEE Trans. Image Process.*, *11*, 670–684.

Starck, J., E. Candès, and D. Donoho (2003), Astronomical image representation by the curvelet transform, *Astron. Astrophys.*, *398*, 785–800.

Zar, J. (1999), *Biostatistical Analysis*, 4th ed., Prentice-Hall, Upper Saddle River, N. J.